Diagn Interv Radiol 2020; 26:95–100
© Turkish Society of Radiology 2020

ABDOMINAL IMAGING
ORIGINAL ARTICLE

Compatibility of true and virtual unenhanced attenuation in rapid kV-switching dual energy CT

İlkay Çamlıdağ

PURPOSE
We aimed to evaluate whether virtual unenhanced images generated from nephrographic phase on rapid kV-switching dual energy computed tomography (rsDECT) can replace true unenhanced images by comparing attenuation values of various intraabdominal structures.

METHODS
In this retrospective study, 142 patients had unenhanced and nephrographic phase DECT images. Attenuation values of the aorta, liver, spleen, pancreas, bilateral renal parenchyma, inferior vena cava, gallbladder and paraspinal muscle on true and virtual unenhanced images were recorded. Frequency of organs that had more than 10 and 20 HU of attenuation difference were also calculated.

RESULTS
A total of 1224 regions of interest were sampled. No statistically significant differences were found between true and virtual unenhanced attenuation of the aorta, spleen and pancreas. The other structures had significant differences ($P < 0.001$). Correlation between measurements were weak to moderate (r, 0.17–0.72). Of the organs, 20% had more than 10 HU difference and 5% had more than 20 HU difference between true and virtual unenhanced images.

CONCLUSION
rsDECT-based virtual unenhanced images do not seem to be an ideal surrogate for true unenhanced images.

Dual energy computed tomography (DECT) has been introduced into clinical practice in 2006 and is being increasingly used in various applications since then. Dual energy technology provides discrimination of materials within a given tissue by taking advantage of the variations of photon absorption at different photon energy levels. To be able to discriminate different materials, which is also named as material decomposition, these materials ideally need to have large atomic number differences such as the iodinated contrast material with high atomic number and soft tissues of the body with low atomic number. Therefore the ability to discriminate and quantify iodine in a given tissue is the major advantage of DECT. Moreover, iodine can be subtracted from the images and virtual unenhanced images can be generated. Virtual monoenergetic images is another application of DECT that can improve lesion conspicuity in lower kV levels (1). The technology of the DECT imaging systems varies based on the X-ray tube and detector designs and each system has their own algorithms to provide material decomposition with their own specific advantages and disadvantages (2–4).

Standard unenhanced images form an essential component of multiphasic CT examinations, particularly in genitourinary conditions such as indeterminate renal mass, hematuria evaluation and adrenal nodule characterization. However, the more phases of imaging are present, the more radiation dose will be given to the patient and if this precontrast phase could be omitted without compromising the diagnostic information, it would be of benefit to the patients in terms of both reducing the radiation dose and eliminating the need for additional imaging work-up in case of incidental lesions. That is why the capability to gen-

From the Department of Radiology (İ.Ç. ✉ *ilkayozaydin@hotmail.com*), Ondokuz Mayıs University, Samsun, Turkey.

Received 23 July 2019; revision requested 19 August 2019; last revision received 11 December 2019; accepted 20 December 2019.

DOI 10.5152/dir.2019.19345

You may cite this article as: Çamlıdağ İ. Compatibility of true and virtual unenhanced attenuation in rapid kV-switching dual energy CT. Diagn Interv Radiol 2020; 26:95–100.

erate virtual unenhanced images has been one of the most intriguing features of DECT.

The potential of virtual unenhanced images to replace true unenhanced images in different phases of abdominal CT examinations has been extensively studied to date, especially on dual source scanners due to their wider availability (5–11). Although majority of these studies suggested a good reliability of virtual unenhanced attenuation (VUA) measurements (6, 8, 9, 11), discrepant results were also present (5, 10). To our knowledge, only two studies performed with dual layer spectral detector CT in arterial and portal venous phase showed good approximation of true unenhanced attenuation (TUA) and VUA (12, 13). Despite being the second most available DECT platform, the number of studies performed with single source rapid kV-switching DECT (rsDECT) is very limited. Mendonça et. al (14) showed good consistency of attenuation values between true and virtual unenhanced images in 50 cases in different acquisition phases. Kaza et al. (15) found good TUA-VUA correlation in both corticomedullary and nephrographic phase but in a limited number of 19 cases (15). However, the final study performed by Borhani et al. (16) in arterial and portal venous phase in 94 cases yielded significant differences in TUA-VUA values. Because of the discrepancy of results and relatively low number of cases in these studies, we aimed to evaluate TUA-VUA consistency of various abdominal organs on rsDECT in a larger number of patients. As many of the clinical indications requiring an unenhanced examination were related to genitourinary conditions, we chose to investigate the nephrographic phase as an essential component of these CT examinations.

Methods

This retrospective study was approved by institutional review board (IRB protocol number: 2019/537) and the requirement for informed consent from patients was waived.

Main points

- There are significant differences between TUA and VUA values of some intraabdominal structures, and attenuation values show weak to moderate correlation.
- Attenuation discrepancies of more than 10 HU are present and can be associated with erroneous interpretation.
- Virtual unenhanced images generated from rsDECT are not an ideal surrogate for true unenhanced images.

Patient selection

Patients who underwent triphasic abdominal multidetector CT (MDCT) consisting of unenhanced, dual energy nephrographic phase and excretory phase imaging between December 2015 and May 2019 for hematuria evaluation or renal lesion characterization were eligible for the study (n=144). Patients with low image quality due to artifacts (n=2) were excluded from the study.

Image acquisition

CT examinations were performed on a rapid kV-switching dual-energy 64-detector MDCT scanner (Discovery CT750 HD scanner, GE Healthcare). Unenhanced images were obtained first using a conventional 120 kVp single energy multidetector CT technique (scan type, helical; detector coverage, 40 mm; slice thickness, 5 mm; interval, 1.25 mm; pitch, 1.375:1; speed, 55; and gantry rotation time, 0.7 s). Nephrographic phase DECT images were acquired at 90 s after the contrast injection (scan type, helical; detector coverage, 40 mm; slice thickness, 2.5 mm; interval, 1.25 mm; pitch, 0.984:1; speed, 39.37; and gantry rotation time, 0.7 s; automatic mA modulation range ,260–600 mA; targeted noise index, 17.25). Images were reconstructed with a standard algorithm and application of 30% adaptive statistical iterative reconstruction (ASIR).

Intravenous contrast material was administered (Iohexol: Omnipaque 350, GE Healthcare) using a standardized weight-based dose injected at 2.5–4.0 cc/s rate for a fixed 30-s injection interval, followed by a 25 cc saline flush. Excretory phase images were part of our institutions' routine imaging protocol and acquired with similar parameters to that of unenhanced images; however, they were not used for this analysis.

Image analysis

Image analyses were made on the dedicated workstation by Gemstone Spectral Image (GSI) software (ADW 2.0, GE Healthcare). For evaluating TUA and VUA, the standard and GSI reformat viewer modes were opened separately and iodine suppressed virtual unenhanced images were generated from 70 keV nephrographic phase images. First, abdominal aorta TUA was measured at the infrahiatal level where the posterior segment of the right liver lobe and medial part of the spleen was in the field of view. The region of interest (ROI) was placed to encompass the aorta lumen as much as possible and atherosclerotic calcifications were avoided when present. The same ROI was placed within the posterior segment of the right liver lobe and then within medial part of the spleen centrally by just moving it without changing the size. The ROI for the pancreas was placed within the distal part of the corpus where the parenchyma was the most compacted. The slice where the kidney parenchyma was thickest was chosen for kidney parenchyma attenuation measurement and the ROIs for both kidneys were placed to encompass the parenchyma as much as possible. When there was a renal tumor, normal parenchyma distant from the tumor was sampled for measurement. For inferior vena cava (IVC) measurement, infrarenal IVC was sampled at its most distended section and the ROI was placed to fit the IVC lumen as much as possible. Gallbladder was sampled from the most superior part of the fundus to obtain a more accurate and homogeneous measurement as the debris inside would layer in the dependent portion of the bladder. Paraspinal muscle was sampled at the first lumbar vertebral level where it was most compact. VUA measurements for each structure were performed on the same slices where TUA measurements were made (Fig. 1). As ROI propagation option was not available between these images, the size and location of the ROI were tried to be kept constant manually. All image analyses were performed by an abdominal radiologist with 5 years of experience. To assess intrareader reliability, a subset of 70 patients were chosen randomly and the measurements were repeated on this subset 8 weeks later. In addition, another reader who was a fourth year radiology resident also performed the same measurements independently and in a blinded manner to evaluate inter-reader reliability.

Statistical analysis

Statistical analysis was performed on SPSS 22.0 software package. Data were presented as mean±standard deviation (SD). Mean attenuation values on true and virtual unenhanced images were compared with paired *t* test. Pearson correlation analysis was performed to evaluate the correlation between TUA and VUA.

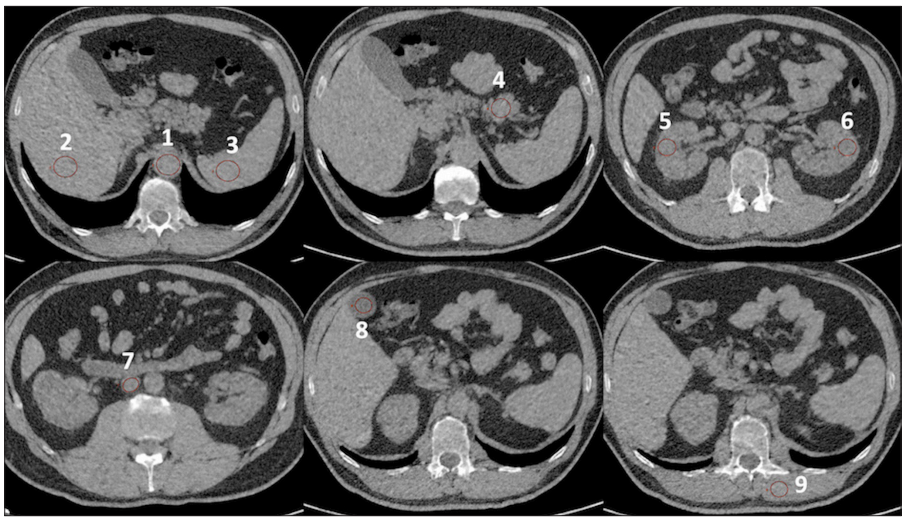

Figure 1. Iodine-suppressed virtual unenhanced images generated from nephrographic phase images show placement of regions of interest on the aorta (1), liver (2), spleen (3), pancreas (4), right kidney (5), left kidney (6), inferior vena cava (7), gallbladder (8), paraspinal muscle (9) and measurement of attenuation values.

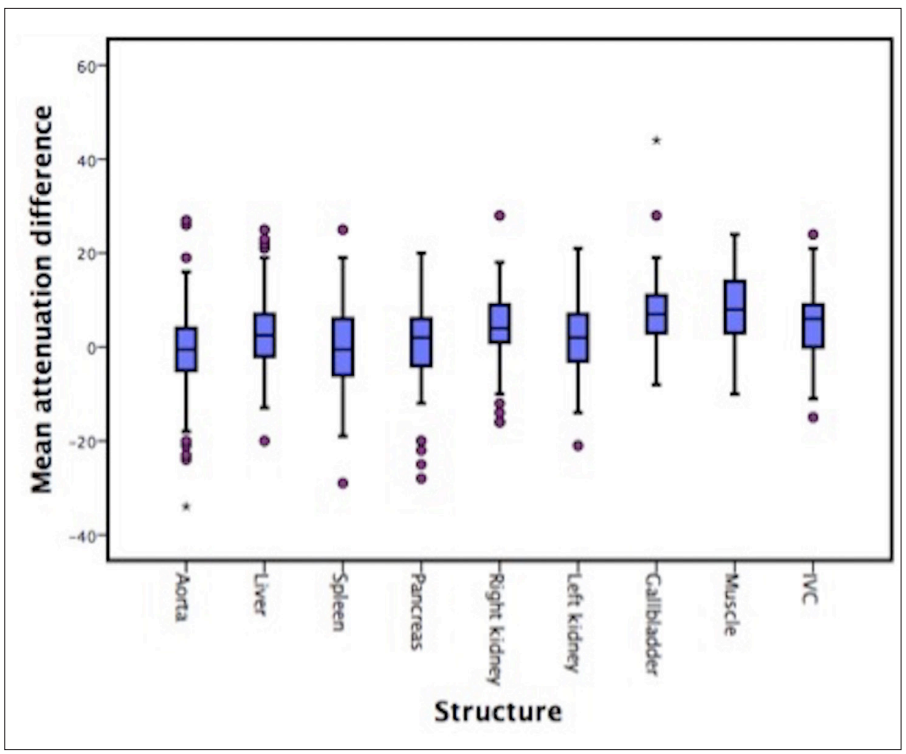

Figure 2. Box-and-whisker plots of the attenuation differences in HU between true and virtual unenhanced images generated from nephrographic phase images. Outliers are indicated by circles and the *asterisks* indicate the extremes.

Bland-Altman analysis was performed to evaluate the magnitude of variation. The frequencies of structures showing 10 and 20 Hounsfield units (HU) of discrepancy between TUA and VUA were calculated. To evaluate intra and inter-reader agreement, intraclass correlation coefficients (ICC) and their 95% confidence intervals were calculated based on single measurement, absolute agreement, 2-way mixed model. Values less than 0.4 were indicative of poor reliability, values between 0.4 and 0.6 indicated moderate reliability, values between 0.6 and 0.75 indicated good reliability and values greater than 0.75 indicated excellent reliability.

The level of statistical significance was set as $P < 0.05$.

Results

A total of 142 patients (92 male, 50 female) were included in this study. In 4 patients with previous right nephrectomy, 2 patients with left nephrectomy and 21 patients with cholecystectomy, measurements were not performed and a total of 1224 ROIs were sampled in all patients. Mean patient age was 61 years (range, 20–86). Mean TUA and VUA for each structure, and the frequencies of structures that show more than 10 and 20 HU of attenuation difference can be found in Table 1. There were no statistically significant differences between TUA and VUA of the aorta, spleen and pancreas. Although mean attenuation difference was less than 8 HU for gallbladder and paraspinal muscle and less than 5 HU for liver, both kidneys and IVC, these differences were significant statistically ($P < 0.001$). Pearson correlation analysis showed that there was significant correlation between TUA and VUA of investigated structures except for the right kidney (r=0.05). However, these correlations were mainly weak to moderate (r, 0.17–0.72). With regard to the attenuation difference between true and virtual unenhanced images, gallbladder was the structure that showed the highest percentage of cases with more than 10 HU difference (39%) followed by right kidney, aorta, IVC, and other structures. The percentage was less than 10% for all structures except gallbladder (16%) when an attenuation difference of more than 20 HU was investigated. Box-whisker plots of the attenuation differences and Bland-Altman plots can be seen in Figs. 2 and 3. ICC values for intra and interrater reliability mainly showed good to excellent agreement in the majority of the measurements ($P < 0.001$) (Table 2).

Discussion

Our study results showed that aorta, spleen and pancreas VUA values had good approximation of TUA values and the rest of the analyzed organs had significant attenuation differences. The mean attenuation difference was less than 5 HU even in the majority of the organs that seemed to have significant differences. However, it was noteworthy that there were considerable proportions of cases showing more than 10 HU and 20 HU attenuation difference in all organs regardless of having good and bad approximation of attenuation values.

Of initial studies performed with first generation dual source DECT, Graser et

Table 1. Mean true and virtual unenhanced attenuation values and frequency of cases showing more than 10 and 20 HU of differences

Structures of interest	TUA Mean±SD	VUA Mean±SD	*P*	r	95% CI for LoA Upper limit	95% CI for LoA Lower limit	>10 HU difference n (%)	>20 HU difference n (%)
Aorta	39.7±9.1	40.2±6	0.48	0.3	17.85	-18.95	32 (22.5)	6 (4)
Liver	60.2±11	57.5±9	<0.001	0.72	18	-12.6	25 (18)	4 (3)
Spleen	48±7.3	48.6±6.4	0.52	0.24	16.24	-17.6	27 (19)	2 (1.5)
Pancreas	38±12	37±9.6	0.07	0.77	16.5	-15.3	21 (15)	3 (2)
Right kidney	40±5.3	35.9±5	<0.001	0.05*	17.9	-9.9	34 (24)	5 (3.5)
Left kidney	38.1±4.9	35.9±6	<0.001	0.17	16.4	-11.8	24 (17)	4 (3)
IVC	41±6.8	36.6±6.7	<0.001	0.41	18.5	-9.7	24 (17)	8 (6)
Gallbladder	16.2±9	9.1±7.4	<0.001	0.67	20.4	-6.2	55 (39)	23 (16)
Muscle	51.5±9.1	43.5±9.2	<0.001	0.69	22.1	-6.1	4 (3)	4 (3)

TUA, true unenhanced attenuation; VUA, virtual unenhanced attenuation; SD, standard deviation; CI, confidence interval; LoA, limits of agreement; HU, Hounsfield units; IVC, inferior vena cava.
* Represents the only correlation coefficient that was not statistically significant.

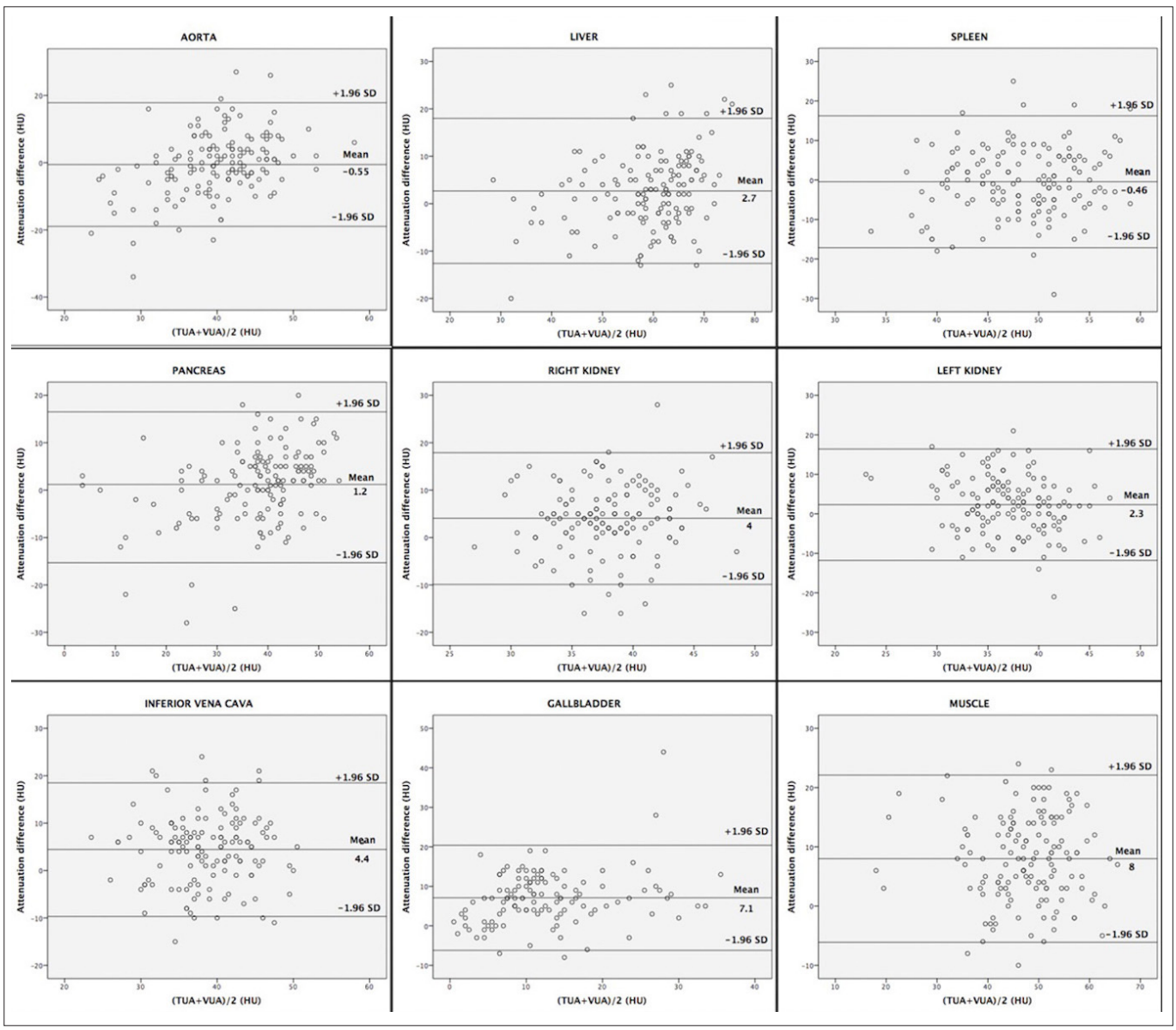

Figure 3. Bland-Altman plots depict the magnitude of differences between TUA and VUA of various intraabdominal structures.

Table 2. Mean intraclass correlation coefficient values for intra and interrater reliability

Structure of interest	Mean intraclass correlation coefficient			
	Intrarater reliability		Interrater reliability	
	TUA	VUA	TUA	VUA
Aorta	0.73	0.73	0.57	0.53
Liver	0.91	0.85	0.69	0.86
Spleen	0.65	0.57	0.58	0.84
Pancreas	0.89	0.85	0.87	0.79
Right kidney	0.69	0.58	0.76	0.69
Left kidney	0.74	0.75	0.75	0.70
IVC	0.60	0.78	0.72	0.54
Gallbladder	0.78	0.80	0.74	0.78
Muscle	0.78	0.80	0.69	0.67

IVC, inferior vena cava; TUA, true unenhanced attenuation; VUA, virtual unenhanced attenuation.

al. (6) found good concordance between TUA and VUA of aorta, liver, bilateral kidneys and psoas muscle in portal venous phase. However, Sahni et al. (10) found significant difference in TUA and VUA of the liver, aorta and renal parenchyma in both nephrographic phase and excretory phase. Of studies performed with second generation dual source DECT, which has a larger second detector coverage and a tin filter technology, Toepker et al. (11) found significant TUA and VUA differences between liver, spleen, aorta, pancreas and muscle, but kidneys, fluids, and muscle did not demonstrate significant differences in arterial and portal venous phases. Kaufmann et al. (8) had similar results to that of Toepker in portal venous phase but muscle attenuation values were significantly different in their study. De Cecco et al. (5) found significant TUA-VUA differences in all organs except for muscle in the arterial phase and muscle, right adrenal, and pancreas in portal venous phase. In studies performed with third generation dual source DECT, which provides a 150 kV tube voltage instead of 140 kV and a thicker tin filter, Durieux et al. (17) had different results in different organs based on the phase of the imaging and type of the dual energy algorithm for generation of virtual unenhanced images. In the study of De Cecco et al. (18), pancreas, renal medulla, adrenal gland, and aorta had significantly smaller VUA values in arterial and portal venous phase. In the only studies performed with dual layer spectral CT systems (12, 13), there was very good compatibility between TUA and VUA values and although there were statistically significant differences in abdominal organs (13), the differences were very small.

Measurement of VUA in HU on rsDECT was not made possible until 2014 because unlike other dual energy platforms, virtual unenhanced images in rsDECT are created in the projection space rather than the image space using material decomposition basis pairs, and virtual unenhanced images are actually water maps which provide the density of water in mg/mL (4). A recently developed multimaterial decomposition algorithm by Mendonca et al. (14) provided material suppressed iodine images which enabled measurement of HU on virtual unenhanced images. This was achieved by removing the iodine and replacing it by the same volume and attenuation of blood that would have been displaced by iodine in the image voxels. Since then only two studies to our knowledge have been performed regarding TUA-VUA compatibility on rsDECT (15, 16). Borhani et al. (16) found excellent correlation between TUA-VUA values but there were significant differences between TUA and VUA values of both kidneys, right adrenal, paraspinal muscle, and aorta in the arterial phase and left kidney and paraspinal muscle in the portal venous phase. Although mean attenuation differences were minimal, there were considerable number of cases who had more than 10 HU attenuation difference. Similarly, Kaza et al. (15) had excellent correlation of attenuation values but showed differences of more than 10 HU in corticomedullary and nephrographic phase. Our study results showed weak to moderate correlation between attenuation values but yielded similar results in terms of differences between TUA and VUA. In total, up to 20% of organs (246/1224) had more than 10 HU difference and 5% (59/1224) had more than 20 HU difference. Strikingly, gallbladder as a cystic structure had the most discrepant attenuation values. This kind of discrepancy could be problematic as it could have caused mischaracterization of a cystic renal lesion as an enhancing tumor or an enhancing renal tumor as a complicated cyst.

The present study has several limitations. Slice thickness and pitch were not identical in unenhanced and nephrographic phase images. The ROI propagation option was not available between true and virtual unenhanced images, therefore the size and location of the ROIs were tried to be kept constant manually. Although most of our study subjects had renal tumors, we did not evaluate the TUA-VUA compatibility of the tumors because it had already been studied in another previously published study of ours regarding the characterization of renal tumors on rsDECT (19) and it was not the primary aim of this study. We did not evaluate adrenal TUA and VUA values although characterization of adrenal lesions are one of the most common indications of an unenhanced CT, because the analyses could have been affected by partial volume averaging and because of the difficulty in ROI placement due to small size. Finally the results of rsDECT cannot be applied to other dual energy platforms.

In conclusion, TUA and VUA compatibility of intraabdominal organs on different dual energy platforms have variable results. Our rsDECT results, performed with the largest number of cases in the literature in nephrographic phase, generally provided significant attenuation differences between organs with discrepancies of more than 10 HU and even 20 HU. Such discrepancies are a significant limitation to the utility of virtual unenhanced images, especially in cystic lesion characterization, and therefore virtual unenhanced images on rsDECT do not seem to be an ideal surrogate for true unenhanced images.

Conflict of interest disclosure

The author declared no conflicts of interest.

References

1. Yeh BM, Shepherd JA, Wang ZJ, Teh HS, Hartman RP, Prevrhal S. Dual-energy and low-kVp CT in the abdomen. AJR Am J Roentgenol 2009; 193:47–54. [CrossRef]

2. Marin D, Boll DT, Mileto A, Nelson RC. State of the art: dual-energy CT of the abdomen. Radiology 2014; 271:327–342. [CrossRef]
3. McCollough CH, Leng S, Yu L, Fletcher JG. Dual- and multi-energy CT: principles, technical approaches, and clinical applications. Radiology 2015; 276:637–653. [CrossRef]
4. Morgan DE. Dual-energy CT of the abdomen. Abdom Imaging 2014; 39:108–134. [CrossRef]
5. De Cecco CN, Darnell A, Macias N, et al. Virtual unenhanced images of the abdomen with second-generation dual-source dual-energy computed tomography: image quality and liver lesion detection. Invest Radiol 2013; 48:1–9. [CrossRef]
6. Graser A, Johnson TR, Hecht EM, et al. Dual-energy CT in patients suspected of having renal masses: can virtual nonenhanced images replace true nonenhanced images? Radiology 2009; 252:433–440. [CrossRef]
7. Haji-Momenian S, Parkinson W, Khati N, Brindle K, Earls J, Zeman RK. Single-energy non-contrast hepatic steatosis criteria applied to virtual non-contrast images: is it still highly specific and positively predictive? Clin Radiol 2018; 73:594.e7–e15. [CrossRef]
8. Kaufmann S, Sauter A, Spira D, et al. Tin-filter enhanced dual-energy-CT: image quality and accuracy of CT numbers in virtual noncontrast imaging. Acad Radiol 2013; 20:596–603. [CrossRef]
9. Lin YM, Chiou YY, Wu MH, Huang SS, Shen SH. Attenuation values of renal parenchyma in virtual noncontrast images acquired from multiphase renal dual-energy CT: Comparison with standard noncontrast CT. Eur J Radiol 2018; 101:103–110. [CrossRef]
10. Sahni VA, Shinagare AB, Silverman SG. Virtual unenhanced CT images acquired from dual-energy CT urography: accuracy of attenuation values and variation with contrast material phase. Clin Radiol 2013; 68:264–271. [CrossRef]
11. Toepker M, Moritz T, Krauss B, et al. Virtual non-contrast in second-generation, dual-energy computed tomography: reliability of attenuation values. Eur J Radiol 2012; 81:e398–405. [CrossRef]
12. Ananthakrishnan L, Rajiah P, Ahn R, et al. Spectral detector CT-derived virtual non-contrast images: comparison of attenuation values with unenhanced CT. Abdom Radiol (NY) 2017; 42:702–709. [CrossRef]
13. Sauter AP, Muenzel D, Dangelmaier J, et al. Dual-layer spectral computed tomography: Virtual non-contrast in comparison to true non-contrast images. Eur J Radiol 2018; 104:108–114. [CrossRef]
14. Mendonca PR, Lamb P, Sahani DV. A flexible method for multi-material decomposition of dual-energy CT images. IEEE Trans Med Imaging 2014; 33:99–116. [CrossRef]
15. Kaza RK, Raff EA, Davenport MS, Khalatbari S. Variability of CT attenuation measurements in virtual unenhanced images generated using multimaterial decomposition from fast kilovoltage-switching dual-energy CT. Acad Radiol 2017; 24:365–372. [CrossRef]
16. Borhani AA, Kulzer M, Iranpour N, et al. Comparison of true unenhanced and virtual unenhanced (VUE) attenuation values in abdominopelvic single-source rapid kilovoltage-switching spectral CT. Abdom Radiol (NY) 2017; 42:710–717. [CrossRef]
17. Durieux P, Gevenois PA, Muylem AV, Howarth N, Keyzer C. Abdominal attenuation values on virtual and true unenhanced images obtained with third-generation dual-source dual-energy CT. AJR Am J Roentgenol 2018; 210:1042–1058. [CrossRef]
18. De Cecco CN, Muscogiuri G, Schoepf UJ, et al. Virtual unenhanced imaging of the liver with third-generation dual-source dual-energy CT and advanced modeled iterative reconstruction. Eur J Radiol 2016; 85:1257–1264. [CrossRef]
19. Camlidag I, Nural MS, Danaci M, Ozden E. Usefulness of rapid kV-switching dual energy CT in renal tumor characterization. Abdom Radiol (NY) 2019; 44:1841–1849. [CrossRef]